The RAVE complex is an isoform-specific V-ATPase assembly factor in yeast

Anne M. Smardon*, Heba I. Diab*, Maureen Tarsio*, Theodore T. Diakov, Negin Dehdar Nasab, Robert W. West, and Patricia M. Kane
Department of Biochemistry and Molecular Biology, SUNY Upstate Medical University, Syracuse, NY 13210

ABSTRACT The regulator of ATPase of vacuoles and endosomes (RAVE) complex is implicated in vacuolar H⁺-translocating ATPase (V-ATPase) assembly and activity. In yeast, *rav1Δ* mutants exhibit a Vma⁻ growth phenotype characteristic of loss of V-ATPase activity only at high temperature. Synthetic genetic analysis identified mutations that exhibit a full, temperature-independent Vma⁻ growth defect when combined with the *rav1Δ* mutation. These include class E *vps* mutations, which compromise endosomal sorting. The synthetic Vma⁻ growth defect could not be attributed to loss of vacuolar acidification in the double mutants, as there was no vacuolar acidification in the *rav1Δ* mutant. The yeast V-ATPase *a* subunit is present as two isoforms, Stv1p in Golgi and endosomes and Vph1p in vacuoles. Rav1p interacts directly with the N-terminal domain of Vph1p. *STV1* overexpression suppressed the growth defects of both *rav1Δ* and *rav1Δvph1Δ*, and allowed RAVE-independent assembly of active Stv1p-containing V-ATPases in vacuoles. Mutations causing synthetic genetic defects in combination with *rav1Δ* perturbed the normal localization of Stv1–green fluorescent protein. We propose that RAVE is necessary for assembly of Vph1-containing V-ATPase complexes but not Stv1-containing complexes. Synthetic Vma⁻ phenotypes arise from defects in Vph1p-containing complexes caused by *rav1Δ*, combined with defects in Stv1p-containing V-ATPases caused by the second mutation. Thus RAVE is the first isoform-specific V-ATPase assembly factor.

Monitoring Editor
Sandra Lemmon
University of Miami

Received: May 3, 2013
Revised: Oct 21, 2013
Accepted: Nov 26, 2013

INTRODUCTION

Vacuolar H^+-translocating ATPases (V-ATPases) are highly conserved proton pumps responsible for acidification of organelles such as mammalian lysosomes, yeast or plant vacuoles, endosomes, Golgi apparatus, and regulated secretory granules in all eukaryotes (Kane, 2006; Forgac, 2007). V-ATPases are multisubunit complexes consisting of a subcomplex of peripheral membrane subunits (V_1) attached to a complex of membrane subunits (V_o). Although higher eukaryotes often encode a number of different tissue- and organelle-specific isoforms, the yeast *Saccharomyces cerevisiae* contains a single set of isoforms (Manolson *et al.*, 1994; Forgac, 2007). *VPH1* encodes the V_o subunit *a* isoform localized predominantly to the vacuole, and *STV1* encodes the second isoform of V_o subunit *a*, present in Golgi and endosomes (Manolson *et al.*, 1992; Kawasaki-Nishi *et al.*, 2001a). Mechanistically, ATP hydrolysis in the V_1 sector is coupled to proton transport through the V_o domain via a rotational mechanism (Hirata *et al.*, 2003). Detachment of V_1 sectors from V_o sectors inactivates both subcomplexes, and serves as a mechanism for regulating V-ATPase activity. Disassembly of the V-ATPase is triggered rapidly by glucose deprivation, and reassembly also occurs rapidly upon glucose readdition (Kane, 2000). There is evidence that Stv1p-containing V-ATPases are less responsive to glucose control than Vph1p-containing complexes (Kawasaki-Nishi *et al.*, 2001b). Regardless of subunit *a* isoform, V-ATPase complexes at the vacuole appear to undergo reversible disassembly more readily than V-ATPases in prevacuolar compartments (Kawasaki-Nishi *et al.*, 2001b; Qi and Forgac, 2007).

The regulator of ATPase of vacuoles and endosomes (RAVE) complex binds to the V_1 complex and subunit C in the cytosol and promotes their assembly with the membrane-bound V_o complex (Seol *et al.*, 2001; Smardon *et al.*, 2002; Smardon and Kane, 2007). In addition to Skp1p, which is found in multiple complexes, including several ubiquitin ligases, the RAVE complex is composed of two

This article was published online ahead of print in MBoC in Press (http://www.molbiolcell.org/cgi/doi/10.1091/mbc.E13-05-0231) December 4, 2013.
*These authors contributed equally to this work.
Address correspondence to: Patricia M. Kane (kanepm@upstate.edu).
Abbreviations used: BCECF-AM, 2′,7′-bis-(2-carboxyethyl)-5-(and-6)-carboxyfluorescein, acetoxymethyl ester; MBP, maltose-binding protein; MES, (2-(*N*-morpholino)ethanesulfonic acid); RAVE, regulator of ATPase of vacuoles and endosomes; SC, fully supplemented minimal medium; SGA, synthetic genetic analysis; V-ATPase, vacuolar H^+-translocating ATPase; YEPD, yeast extract–peptone–dextrose.

other proteins, Rav1p and Rav2p (Seol *et al.*, 2001). Biochemical approaches have revealed that Rav1p is the central component of the RAVE complex, with distinct binding sites for Rav2p, Skp1p, V_1 subunits E and/or G, and V_1 subunit C (Smardon *et al.*, 2002; Smardon and Kane, 2007). Deletion of either *RAV1* or *RAV2* results in defective assembly of V-ATPase complexes at the vacuole, and both biosynthetic assembly of V-ATPases and reassembly of complexes disassembled in response to glucose deprivation were affected in the *rav1Δ* mutant (Seol *et al.*, 2001; Smardon *et al.*, 2002). Interestingly, the yeast *rav1Δ* and *rav2Δ* mutants both exhibit a "partial" Vma^- phenotype, with the characteristic Vma^- growth defects at high pH and high Ca^{2+} concentrations only observed at 37°C. The source of this temperature sensitivity is not well understood (Seol *et al.*, 2001). Loss of RAVE function has also been reported to compromise transport between early endosomes and the prevacuolar compartment (Sipos *et al.*, 2004).

RAV1 homologues exist in higher eukaryotes as well, in which they are called rabconnectin-3α or DMX-like proteins (Kraemer *et al.*, 1998; Nagano *et al.*, 2002). Only fungi have homologues of yeast *RAV2*, but higher eukaryotes do have a second rabconnectin subunit (rabconnectin-3β) that forms a complex with rabconnectin-3α and gives identical phenotypes to rabconnectin-3α when disrupted (Sakisaka and Takai, 2005; Yan *et al.*, 2009). In *Drosophila* and human cell lines, rabconnectin3-α and rabconnectin3-β have been implicated in regulation of organelle acidification and endosomal trafficking (Yan *et al.*, 2009; Sethi *et al.*, 2010). Loss of rabconnectin-3 function in these organisms is associated with Notch signaling defects that have been traced to a requirement for endosomal acidification in this signaling pathway (Yan *et al.*, 2009; Sethi *et al.*, 2010). In zebrafish, loss of rabconnectin function is associated with reduced acidification of synaptic vesicles and release of V_1 subunits from membranes in hair cells (Einhorn *et al.*, 2012). Taken together, the data suggest that RAVE/rabconnectins have a conserved function in vacuolar acidification, with Rav1p and its homologues playing a central role in this function.

To better understand RAVE function, we undertook genetic analysis in yeast, seeking mutants that require Rav1p function for normal growth and viability. Mutations in several class E *vps* genes (Raymond *et al.*, 1992), which encode components of the ESCRT (endosomal sorting complex required for transport) complexes of the multivesicular body and other accessory proteins (Katzmann *et al.*, 2003; Bowers *et al.*, 2004), resulted in poor growth in combination with a *rav1Δ* mutation, and further analysis showed that the combined mutations result in a synthetic Vma^- phenotype. This synthetic phenotype does not arise from further alkalinization of the vacuole, because the *rav1Δ* mutant proved to have an alkaline vacuolar pH that was similar to the double mutant. Instead, we propose that the synthetic phenotype arises from an isoform-specific requirement for Rav1p in assembly of Vph1-containing V-ATPase complexes at the vacuole, combined with an effect of the class E *vps* mutants on Stv1-containing V-ATPase complexes.

RESULTS

rav1Δ mutations show a synthetic Vma^- phenotype in combination with class E *vps* mutations

Genome-level synthetic genetic analysis (SGA) has emerged as a powerful method for placing gene products in their cellular and physiological context (Tong *et al.*, 2001; Costanzo *et al.*, 2010). We constructed a mutant strain containing a *rav1Δ::natMX* allele and then mated it to a library of nonessential haploid deletion strains as described in *Materials and Methods*. Diploids were selected and sporulated, and double-mutant haploid disruptants were selected as described by Tong *et al.* (2001). Strains that failed to grow on the haploid double-mutant selection plate but that did grow on the haploid single (library)-mutant selection plate were identified by visual inspection as candidate mutations that cause negative synthetic growth phenotypes with the *rav1Δ* mutation. More than 80 candidate mutations (Supplemental Table S1) were identified in at least two of three independent screens. Gene ontology (GO) analysis was performed on the candidate genes (Robinson *et al.*, 2002). Biological process GO terms having the highest significance were "protein transport" (p value = 3.2×10^{-10}) and "vacuolar/lysosomal transport" (p value = 3.6×10^{-9}), and the most significant cellular component terms were "endosome membrane" and "endosome" (both with p values $<1 \times 10^{-14}$). Other significant GO terms are listed in Table S2.

Other screens have also identified *rav1Δ* synthetic genetic interactions (Costanzo *et al.*, 2010). The ~50 deletion mutations reported on the yeast BioGRID 3.2 database (Chatr-Aryamontri *et al.*, 2013) as having negative genetic, synthetic growth, or synthetic lethal interactions with *rav1Δ* were compared with results of our SGA screen. Ten of the previously identified mutations were also found in our SGA screen (Table S1). GO analysis of the full set of previously identified genes revealed "retrograde transport, endosome to Golgi" as the most significant hit in the GO biological process category (p value = 1.8×10^{-9}), and "Golgi apparatus" as the highest significant hit in the GO cellular component category (p value = 1.6×10^{-10}). The RAVE complex has been implicated in endosomal and lysosomal acidification and Golgi to endosome trafficking, so despite limited overlap in the specific genes, it appears that both our SGA screen and the previous screens have identified mutations with related GO terms.

Recent high-throughput SGA screens have quantitated synthetic growth defects by computational analysis of colony size of single and double mutants (Costanzo *et al.*, 2010). Because our initial genomic screen relied on a more qualitative analysis, we sought to confirm a number of the negative growth interactions through tetrad dissection on yeast extract–peptone–dextrose medium (YEPD) buffered to pH 5 (Table 1). These conditions are fully permissive for the *rav1Δ* mutation, so we reasoned that any effects of the mutation on germination or growth of the spores would be suppressed. We obtained viable double-mutant spores for most crosses by this method and then examined their growth under more stressful conditions. In a number of cases, when these spores were subjected to higher pH and higher calcium concentrations, synthetic growth defects were revealed, supporting a genetic interaction of the candidate mutation with *rav1Δ*. Interestingly, one class of mutations that was prominent in our screen but not in previous SGA screens was the class E *vps* mutants (Table 1). In addition to confirming the interactions with several class E *vps* mutants observed in the initial screen, we also identified synthetic growth phenotypes with a number of additional class E *vps* mutants (Table 1). Sensitivity to elevated pH and calcium at all temperatures is a signature phenotype of the *vma* mutants, which lack all V-ATPase activity (Kane, 2007). The *rav1Δ* mutant is tolerant of high pH and elevated (60 mM) extracellular calcium at 30°C. Most of the class E *vps* mutants also tolerated these conditions. In contrast, almost all of the class E *vps rav1Δ* double mutants were unable to grow on YEPD, pH 7.5 medium containing 60 mM $CaCl_2$ at 30°C, although their growth was comparable with the single mutants on YEPD, pH 5. Representative mutants are shown in Figure 1, but a very similar phenotype was observed with the *rav1Δvps36Δ*, *rav1Δvps25Δ*, and *rav1Δsnf7Δ* mutants as well. Therefore many of the class E *vps* mutations produce a synthetic Vma^- growth phenotype when combined with *rav1Δ*. Many of the

Gene	Aliases	Confirmed phenotype with *rav1Δ*?	Proposed role
DID4	*VPS2, REN1, GRD2, CHM2*	Synthetic Vma$^-$	ESCRT III complex
SRN2	*VPS37*	Synthetic Vma$^-$	ESCRT I complex
VTA1		Not confirmed	Regulates ESCRT recycling via Vps4p
VPS60	*MOS10, CHM5*	Weak synthetic Vma$^-$	Interacts with VTA1, regulates Vps4p
DID2		Not confirmed	Regulates Vps4p
VPS24	*DID3*	Synthetic Vma$^-$	ESCRT III complex
VPS27	*GRD11, DID7, SSV17*	Very weak synthetic Vma$^-$	ESCRT 0 complex
VPS28		Synthetic Vma$^-$	ESCRT I complex
VPS4	*CSC1, END13, GRD13, DID6, DOS1, MUT4, NPI2, SSV7, UBP4*	No synthetic phenotype[a]	Recycles ESCRT complexes
DOA4		Weak synthetic Vma$^-$	Deubiquitinating enzyme, recycles ubiquitin
RIM20		Synthetic Vma$^-$	Associates with *SNF7* at MVB
VPS36[b]	*GRD12, VAC3*	Synthetic Vma$^-$	ESCRT II complex
VPS23[b]	*STP22*	Synthetic Vma$^-$	ESCRT I complex
SNF7[b]	*DID1, VPS32, RNS4*	Synthetic Vma$^-$	ESCRT III complex
VPS25[b]		Synthetic Vma$^-$	ESCRT II complex

[a]The *vps4Δ* single mutation appeared to cause a fairly strong Vma$^-$ phenotype, and there was no further growth inhibition in the double mutant.
[b]These genes were not identified as interactors in the original screen (Supplemental Table 1) but were tested by tetrad dissection for interactions with *rav1Δ*.

TABLE 1: Class E vps genes with potential genetic interactions with *rav*1*Δ*.

class E *vps* mutations define a series of ESCRT complexes, which are involved in identification and transfer of ubiquitinated cargo into intralumenal vesicles at the multivesicular body (Hurley and Emr, 2006). The class E *vps* mutants that yielded synthetic Vma$^-$ phenotypes in Table 1 include members of all three of the ESCRT complexes, as well as a number of other accessory proteins acting at the multivesicular body (Bowers *et al.*, 2004).

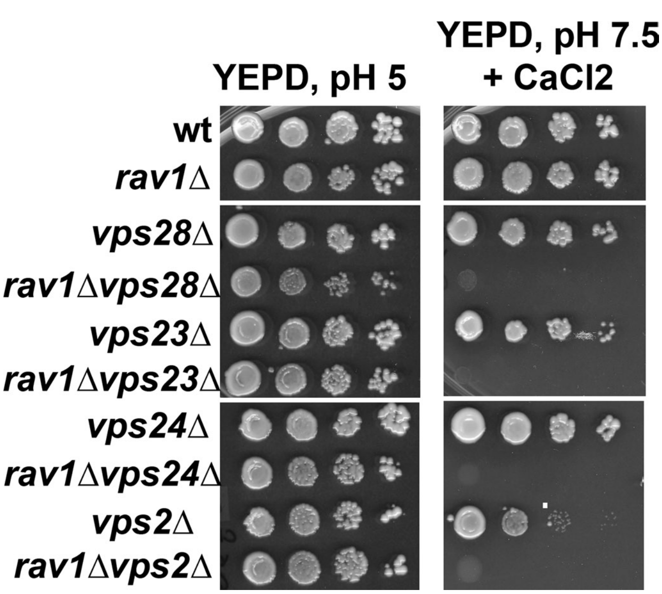

FIGURE 1: Synthetic growth defects of *rav1Δ* and class E *vps* mutants. The indicated strains were grown to log phase in YEPD, pH 5; diluted to an OD_{600} of 0.5 in the same medium; and then serially 10-fold diluted in a microtiter plate. Cells were transferred to YEPD, pH 5 and grown for 3 d at 30°C or to YEPD, pH 7.5 + 60 mM $CaCl_2$ plates and grown for 5 d at 30°C.

Effects of *rav1Δ* and *rav1Δ* class E *vps* double mutants on vacuolar pH

It has previously been suggested that V-ATPases destined for the vacuole are partially retained in a prevacuolar compartment in class E *vps* mutants (Piper *et al.*, 1995), and significant defects in V-ATPase activity in isolated vacuoles from *rav1Δ* mutants have also been reported (Smardon *et al.*, 2002; Smardon and Kane, 2007). The synthetic Vma$^-$ phenotype of the double *rav1Δ* class E *vps* mutants might arise from synergistic defects in vacuolar acidification in these mutants, resulting in vacuolar alkalinization beyond that of the *rav1Δ* mutant. Therefore we measured vacuolar pH using the ratiometric pH-sensitive dye BCECF-AM in the *rav1Δ* mutant, a class E *vps24Δ* mutant, and a *vps24Δrav1Δ* double mutant to determine whether the double mutants showed a more pronounced vacuolar alkalinization than either single mutant. The cleaved BCECF localizes to the vacuole. Both overall cellular and vacuolar pH control are compromised by glucose deprivation, but readdition of glucose to wild-type cells briefly deprived of glucose results in a characteristic drop in vacuolar pH that is dependent on V-ATPase activity (Martinez-Munoz and Kane, 2008), as observed in Figure 2A. The *vps24Δ* mutant shows a vacuolar pH response to glucose very similar to that of wild-type cells, suggesting that there is no significant defect in vacuolar acidification. In contrast, the vacuolar pH sharply increases upon glucose addition in the *rav1Δ* mutant. Similar behavior is observed in other mutants lacking V-ATPase activity, including the *vph1Δ* mutant (Tarsio *et al.*, 2011). This increase has been attributed to glucose activation of cellular proton export that is not balanced by proton import into the vacuole when V-ATPase activity is lacking (Martinez-Munoz and Kane, 2008). The vacuolar pH also increases upon glucose addition to the *rav1Δvps24Δ* mutant, although the increase is not as pronounced as in the *rav1Δ* single mutant. Importantly, these results are not consistent with vacuolar alkalinization as the basis of the synthetic growth defects seen in the double mutant.

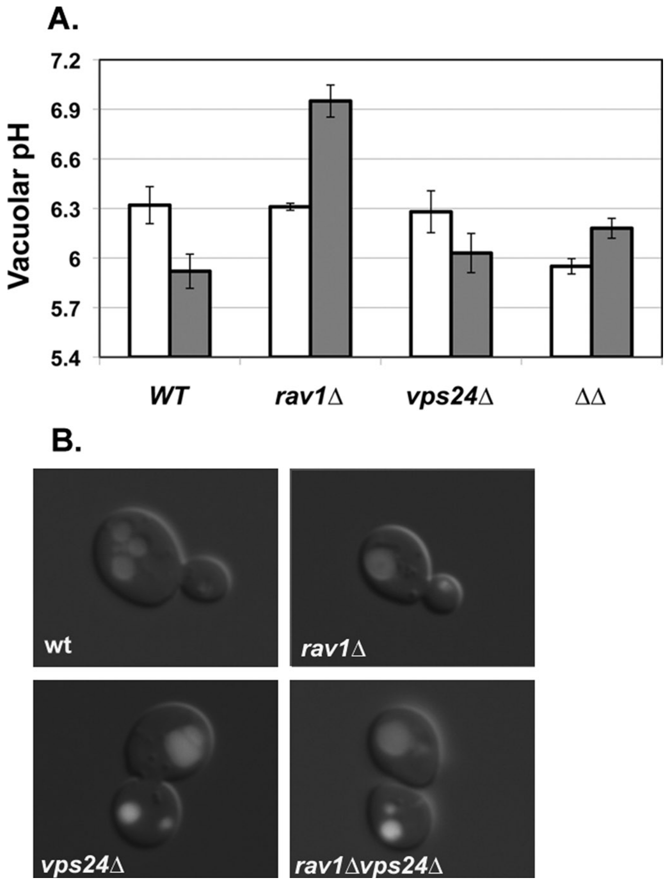

FIGURE 2: Vacuolar pH responses are normal in *vps24Δ*, but defective in both *rav1Δ* and *rav1Δvps24Δ*. (A) Vacuolar pH was measured after a brief glucose deprivation (white bars) and five minutes after glucose readdition (gray bars) in the indicated strains, after loading with the ratiometric fluorescent pH indicator BCECF-AM (see *Materials and Methods*). The mean of three independent experiments is shown; error bars correspond to SEM. (B) Vacuolar localization of BCECF in all of the strains was confirmed by fluorescence microscopy. BCECF was imaged using fluorescein optics, and fluorescence images are superimposed on differential interference contrast (DIC) images, in which the vacuole(s) appears as an indentation(s).

We also noted in Figure 2A that the initial vacuolar pH after glucose deprivation is somewhat lower in the *rav1Δvps24Δ* mutant than in wild-type cells. Given the strong Vma phenotype of this mutant, this was somewhat surprising. However, multiple aspects of cellular pH homeostasis are impacted by glucose deprivation, and Pma1 mislocalization (see Figure 6B later in this article) can compound this (Tarsio *et al.*, 2011). The response to glucose readdition is a more direct reflection of V-ATPase activity, and this response is compromised in both the *rav1Δ* and *rav1Δvps24Δ* mutant.

Because we observed wild-type vacuolar pH responses in the *vps24Δ* mutant, even though it has been suggested that vacuolar acidification is compromised in class E *vps* mutants (Raymond *et al.*, 1992), we confirmed vacuolar localization of BCECF in the mutants in Figure 2B. The vacuole is visualized as an indentation under Nomarski optics, and BCECF fluorescence localizes to the vacuole in all four mutants. Therefore vacuolar fluorescence is likely the major contributor to the population-based pH measurements in Figure 2A.

Does loss of RAVE function specifically affect Vph1p-containing V-ATPases?

The results in Figure 2 suggest that the *rav1Δ* mutant phenotype resembles certain phenotypes of the *vph1Δ* mutant. The partial Vma⁻ phenotypes of the *vph1Δ* mutant, compared with other *vma* mutants, have been attributed to activity of V-ATPases containing the second *a* subunit isoform Stv1p (Manolson *et al.*, 1994). We hypothesized that if the partial Vma⁻ phenotype of *rav1Δ* comes primarily from loss of Vph1p function, then Stv1p may be functional in the absence of RAVE. Growth phenotypes of a *vph1Δ* mutant are suppressed by overexpression of *STV1* (Manolson *et al.*, 1994). If Stv1p-containing complexes can assemble in the absence of RAVE, then *STV1* overexpression might also suppress the growth phenotypes of a *rav1Δ* mutant. As shown in Figure 3A, the poor growth of a *rav1Δ* mutant on YEPD, pH 7.5 medium at 37°C is suppressed by overexpression of *STV1*. This suppression does not depend on the presence of Vph1p, because poor growth of a *rav1Δvph1Δ* mutant can also be suppressed by overexpression of hemagglutinin (HA) epitope–tagged *STV1*. This result suggests that Stv1p-containing V-ATPases can assemble and function in the absence of RAVE.

Because pure Golgi and endosomal fractions are difficult to isolate from yeast, the biochemical properties of Stv1p-containing V-ATPases have generally been assayed by overexpressing *STV1*. Under these conditions, Stv1p is transported to the vacuole and assembles into V-ATPase complexes, and vacuolar vesicles can be readily isolated and characterized (Manolson *et al.*, 1994; Kawasaki-Nishi *et al.*, 2001b; Qi and Forgac, 2007; Finnigan *et al.*, 2011). To test for RAVE-independent assembly of Stv1p-containing V-ATPase complexes, we isolated vacuolar vesicles from *rav1Δ* mutants with and without overexpression of HA-tagged Stv1p. As shown in Figure 3B, *rav1Δ* mutants have very low V-ATPase activity, but overexpression of *STV1* results in a 10-fold increase in V-ATPase activity, reaching ~30% of the wild-type V-ATPase activity. In Figure 3C, the levels of peripheral V_1 subunits A, B, and C and integral membrane V_o *a* subunits, HA-tagged Stv1p and Vph1p, were compared in vacuolar vesicles isolated from wild-type cells, and the *rav1Δ* mutant with and without *STV1* overexpression. HA-tagged Stv1p is only detected in the vacuoles from the strain containing the overexpression plasmid, as expected. The levels of V_1 subunits, and particularly V_1 subunit C, are low in vacuoles from the *rav1Δ* strain, as reported previously (Smardon and Kane, 2007), but are increased to near wild-type levels in the strain overexpressing HA-tagged Stv1p. Taken together, these results indicate that the increased V-ATPase activity in the *STV1*-overexpressing strain arises from increased assembly of V_1 and V_o subunits and that this assembly occurs in the absence of RAVE function. Although *rav1Δ* mutants have previously been shown to have wild-type levels of Vph1p in isolated vacuoles (Smardon and Kane, 2007), the levels of this subunit appeared to be somewhat higher in the three independent preparations of *rav1Δ* mutant vacuoles shown in Figure 3C than in vacuoles from the wild-type and *rav1Δ* strain overexpressing *STV1*. We assessed the cellular Vph1p levels in whole-cell lysates from wild-type and *rav1Δ* cells with and without *STV1* overexpression in Figure 3D. All of the strains contain comparable amounts of Vph1p. V_1 subunits have been shown previously to be present at comparable levels in wild-type and *rav1Δ* mutants (Smardon *et al.*, 2002; Smardon and Kane, 2007), as shown for V_1 subunit B in Figure 3D. Taken together, the results in Figure 3 indicate that increased V-ATPase activity in vacuoles from *rav1Δ* cells overexpressing *STV1* is supported by an increased ratio of V_1 to V_o subunits at the vacuole. Thus V-ATPases are able to assemble with the Stv1-HA isoform in the absence of RAVE function.

RAVE has been shown to interact with V_1 subunits and assembled V_1 complexes (Seol *et al.*, 2001; Smardon *et al.*, 2002). There

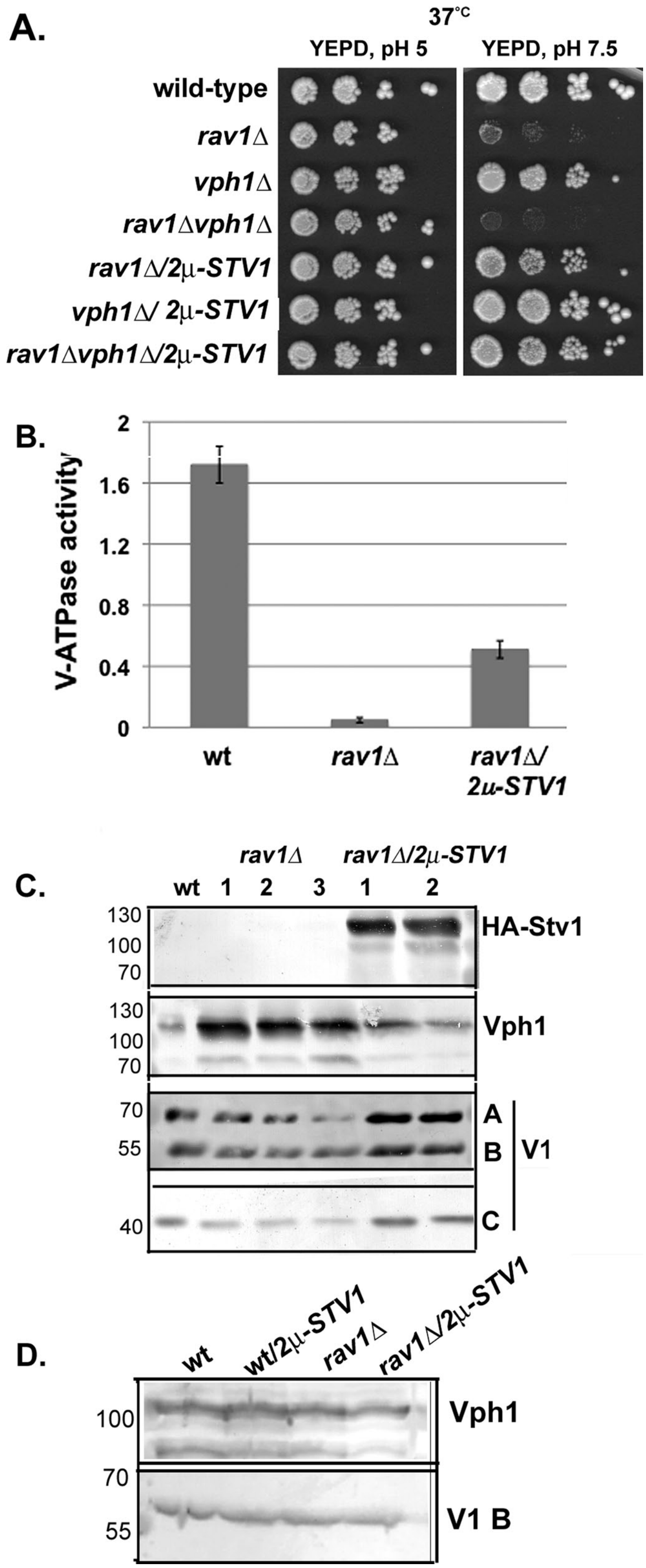

FIGURE 3: *STV1* overexpression suppresses *rav1Δ* growth defects and allows RAVE-independent assembly of V-ATPase complexes at the vacuole. (A) Growth of the indicated strains was compared as described in Figure 1, except that the cells were grown on YEPD, pH 5 and YEPD, pH 7.5 plates at 37°C. (B) Vacuolar vesicles were isolated from wild-type (BY4741), Y3656 *rav1Δ* cells with no plasmid (*rav1Δ*) or Y3656 *rav1Δ* cells transformed with a 2-micron plasmid containing HA-*STV1* (*rav1Δ/HA-STV1*). V-ATPase–specific activity was measured for three independent preparations of vacuolar vesicles, and the mean ± SEM is shown. (C) Samples for one to three independent vacuole preparations from each strain were separated by SDS–PAGE and subjected to immunoblotting with the indicated antibodies. Identical amounts of vacuolar protein from each sample were loaded for comparison. Blots were probed with anti-HA to identify HA-Stv1p, and with monoclonal antibodies against Vph1p and V_1 subunits A, B, and C. The positions of molecular mass markers (mass in kDa) are indicated on the right. (D) Whole-cell lysates were prepared from the indicated strains and separated by SDS–PAGE, and immunoblots were probed with the same antibodies used in (C). Loads were normalized to an equivalent number of lysed cells.

are no subunit isoforms of the yeast V_1 subunits, so these interactions cannot readily account for the differing RAVE dependence of Stv1p- and Vph1p-containing V-ATPase complexes. Therefore we tested whether Vph1p and/or Stv1p also interact with RAVE. The largest cytosolically exposed portion of the V_o sector is the soluble N-terminal domain of Vph1p or Stv1p (Vph1NT and Stv1NT; Kawasaki-Nishi *et al.*, 2001a; Benlekbir *et al.*, 2012; Oot and Wilkens, 2012). We tested whether Vph1NT and Stv1NT are able to interact with Rav1p by two-hybrid assay. In this version of the assay, the *ADE2* and *HIS3* genes are under control of the *GAL* promoter, so growth on medium lacking adenine and histidine indicates that a two-hybrid interaction has occurred. As shown in Figure 4, there is no growth on medium lacking adenine and histidine when the *RAV1* two-hybrid construct is combined with the activation domain with no fusion partner (pACT), or with the Stv1-NT fusion construct. However, Rav1p combined with Vph1NT does support growth, suggesting that Rav1p is able to interact with Vph1NT. All three strains grow on medium lacking both tryptophan and leucine (–Trp, –Leu), indicating that both plasmids were present in all three strains. These results indicate for the first time that RAVE may interact with the V_o sector of the V-ATPase during reassembly of V_1 with V_o and may show a preference for Vph1p over Stv1p.

To address whether Vph1NT binds directly with Rav1p, we expressed and purified the most highly conserved region of *RAV1* (corresponding to amino acids 840–1125) as a glutathione *S*-transferase fusion (GST-Rav1(840–1125)) from *Escherichia coli*. A FLAG-tagged version of Vph1NT was also expressed and purified, and both proteins are shown in the top panel of Figure 5A. We then bound the purified GST-Rav1(840–1125) to glutathione Sepharose, washed the beads, and added Vph1NT-FLAG to the beads. After being washed, GST-Rav1(840–1125) was eluted with excess glutathione, and we looked for coelution of bound Vph1NT-FLAG. As shown in the top panel of Figure 5A, Vph1NT-FLAG coelutes with GST-Rav1(840–1125) at substoichiometric levels. We confirmed the identity of the eluted Vph1NT-FLAG by Western blotting (bottom panel of Figure 5A). Figure 5B shows that no Vph1NT-FLAG bound to the column in the absence of GST-Rav1(840–1125). These experiments indicate that Vph1NT interacts directly with the most highly conserved region of Rav1p. We attempted to conduct the same experiment with Stv1NT-FLAG, but the bacterially expressed Stv1NT-FLAG tended to aggregate and bound to the glutathione beads in the absence of GST-Rav1(840–1125). Therefore we can conclude that this region of Rav1p is capable of binding to Vph1NT directly, but cannot conclude that it provides specificity for Vph1NT over Stv1NT.

Do synthetic phenotypes with *rav1Δ* indicate compromised function of Stv1p-containing V-ATPases?

If Stv1p-containing V-ATPases assemble in the absence of RAVE, then it is possible that the activity of these complexes is responsible

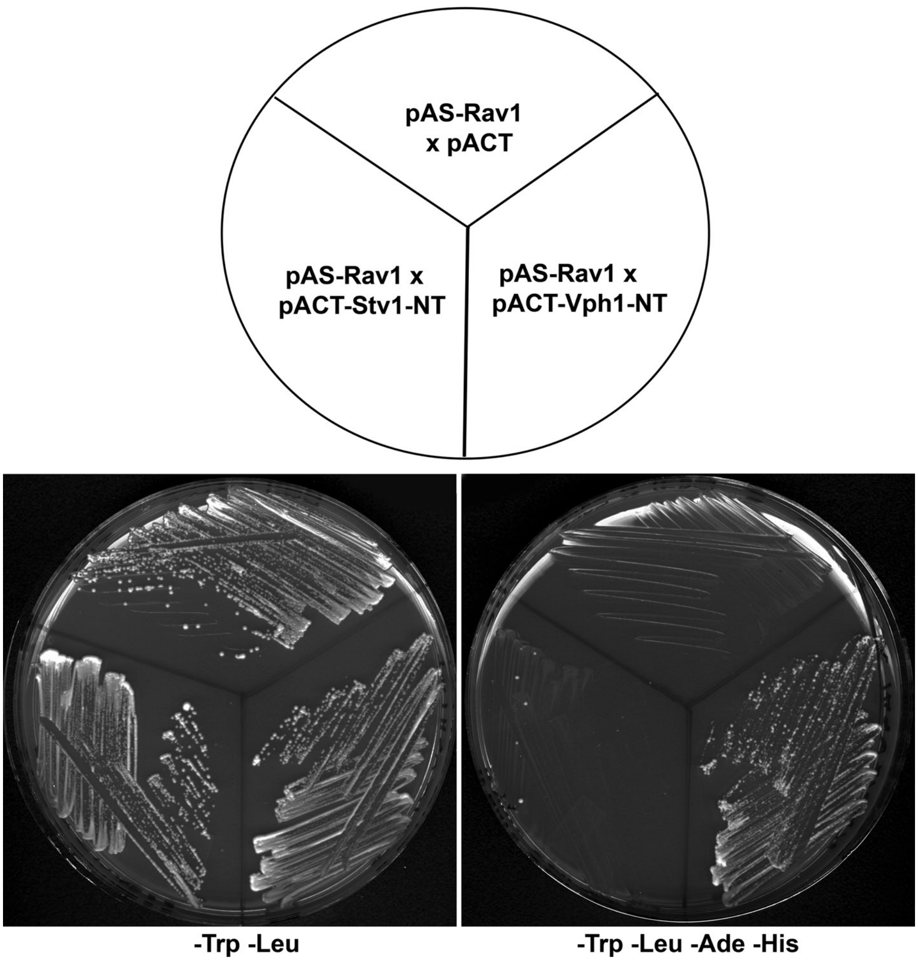

FIGURE 4: Two-hybrid interaction of *RAV1* and *VPH1-NT*. Cells containing pAS-RAV1 were mated to cells containing pACT, pACT-Stv1NT, and pACT-Vph1NT. Growth of the diploids on SC –Trp, –Leu medium, which selects for the plasmids but does not require a two-hybrid interaction, and growth on SC –Trp –Leu –His –Ade medium, which does require a two-hybrid interaction for growth, are compared.

for the relatively mild Vma phenotype of *rav1Δ* mutants. We tested whether the *rav1Δstv1Δ* mutants exhibit a synthetic Vma⁻ growth phenotype, even though the *stv1Δ* mutant was not identified in the SGA screen. As reported previously, the *stv1Δ* single mutant has no Vma⁻ growth phenotype (Manolson *et al*., 1994). However, as shown in Figure 6A, the *rav1Δstv1Δ* mutant is unable to grow on YEPD, pH 7.5 plates at 30°C, indicating there is a strong synthetic Vma⁻ interaction between the two mutations. In fact, as shown in Figure 6A, this interaction appears to be comparable in strength with the well-established synthetic interaction between *vph1Δ* and *stv1Δ* (Manolson *et al*., 1994).

This result suggests that mutations exhibiting a synthetic Vma⁻ phenotype in combination with the *rav1Δ* mutation could affect Stv1p function. It is difficult to directly measure V-ATPase activity in compartments other than the vacuole, but localization of the plasma membrane proton pump Pma1p can provide an indirect assessment of defective V-ATPase activity in these organelles. Loss of V-ATPase activity impacts overall pH homeostasis as well as vacuolar pH (Martinez-Munoz and Kane, 2008). One source of this impact is a reduction in the levels of the major plasma membrane H^+ export pump Pma1p at the membrane and the appearance of the pump in intracellular compartments, including the vacuole (Martinez-Munoz and Kane, 2008; Tarsio *et al*., 2011). The internalized Pma1p is ultimately degraded in the vacuole and does not contribute to vacuolar acidification (Martinez-Munoz and Kane, 2008) but may improve overall pH balance. Interestingly, Pma1p is not internalized in a *vph1Δ* mutant, which has no vacuolar acidification, or in an *stv1Δ* mutant, but is internalized in a *vph1Δstv1Δ* double mutant (Tarsio *et al*., 2011). This suggests that Pma1p internalization requires loss of acidification in organelles other than the vacuole and thus reflects loss of V-ATPase function in these other compartments. We localized Pma1p in the single *rav1Δ* and *vps24Δ* mutants as well as the double *rav1Δvps24Δ* mutant by immunofluorescence microscopy. As shown in Figure 6B, Pma1p is present at the plasma membrane in wild-type cells, the *rav1Δ* mutant, and the *vps24Δ* mutant. However, Pma1p staining at the plasma membrane is reduced in the double *rav1Δvps24Δ* double mutant, and intracellular spots of Pma1p appear, often as one to two dots adjacent to the vacuole. *vma* mutants show a similar pattern of internal Pma1p staining, particularly in strains that contain the full complement of vacuolar proteases (Martinez-Munoz and Kane, 2008; Tarsio *et al*., 2011). The synthetic effect on Pma1p localization in the *rav1Δvps24Δ* double mutant thus resembles the synthetic effect in *vph1Δstv1Δ* mutants. As in the *vph1Δ* mutants, Stv1p must support sufficient organelle acidification in nonvacuolar compartments to sustain normal Pma1p localization in the *rav1Δ* mutant, but this is lost in the *rav1Δvps24Δ* mutant.

The results in Figure 6B indicate that loss of class E *vps* function may compromise function of Stv1p-containing V-ATPases. In fact, HA-tagged Stv1 was previously shown to accumulate in the class E compartment of *vps27Δ* cells (Kawasaki-Nishi *et al*., 2001a), and more recently, a requirement of retrograde transport from endosome to Golgi for normal Stv1p–green fluorescent protein (Stv1p-GFP) localization was demonstrated (Finnigan *et al*., 2011). We compared the localization of Stv1p-GFP in wild-type cells, *vps24Δ*, *rav1Δ*, and *rav1Δvps24Δ* mutants by fluorescence microscopy (Figure 7). As reported previously, Stv1p-GFP in wild-type cells localizes to multiple cytosolic puncta (Finnigan *et al*., 2011, 2012). A similar distribution was seen in *rav1Δ* mutants. The *vps24Δ* mutant showed increased staining in one to two large dots adjacent to the vacuole, similar to the class E compartment described previously in class E *vps* mutants (Raymond *et al*., 1992), and fewer cytosolic puncta. These results are consistent with previous data indicating that mutations in the class E *vps* genes trap Stv1-GFP in the aberrant class E compartments (Finnigan *et al*., 2011, 2012). The *rav1Δvps24Δ* mutant shows a similar Stv1-GFP distribution to the *vps24Δ* strain. These results indicate that the synthetic growth defects of the *rav1Δ* class E *vps* double mutants may arise from combined effects of the *rav1Δ* mutation disabling Vph1-containing V-ATPases at the vacuole and the class E *vps* mutation altering distribution of Stv1-containing V-ATPases in compartments other than the vacuole.

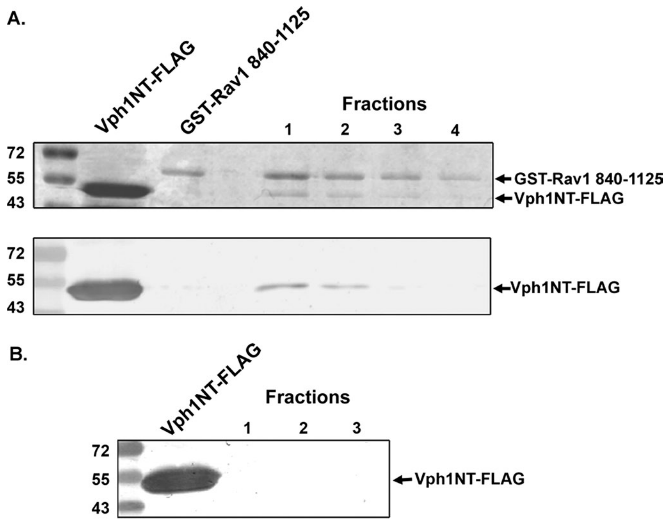

FIGURE 5: Direct interaction of expressed Vph1NT-FLAG and GST-Rav1(840–1125). (A) Coomassie-stained gel (top) and immunoblot probed with anti-Vph1p (bottom) are shown. Purified Vph1NT-FLAG and GST-Rav1(840–1125) were loaded in lanes 2 and 3. Fractions 1–4 correspond to fractions eluted from glutathione resin incubated with both proteins after addition of excess reduced glutathione, as described in *Materials and Methods*. (B) The same experiment was conducted in the absence of GST-Rav1(840–1125) to confirm Rav1-dependent binding of Vph1NT to the resin. Purified Vph1NT-FLAG was loaded in lane 2, and fractions 1–3 correspond to fractions eluted from glutathione resin and visualized by immunoblotting with anti-Vph1p antibody. Sizes of molecular mass markers in lane 1 are shown at left.

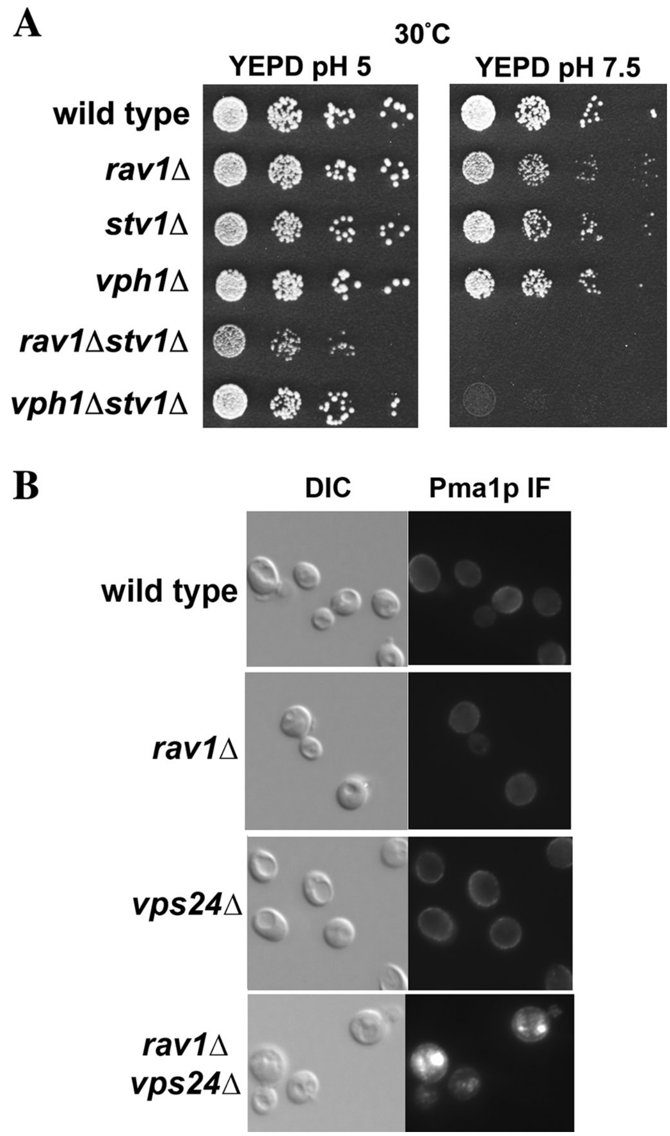

FIGURE 6: Mutations showing synthetic phenotypes in combination with *rav1*Δ may affect Stv1p function. (A) Wild-type (BY4741), Y3656 *rav1*Δ, BY4741 *stv1*Δ, BY4741 *vph1*Δ, BY4741 *rav1*Δ*stv1*Δ, and BY4741 *vph1*Δ*stv1*Δ mutants were serially diluted from log-phase liquid cultures of comparable density, then plated on YEPD, pH 5 and YEPD, pH 7.5 plates. Growth after 2 d at 30°C is shown. (B) Pma1p was localized by indirect immunofluorescence, as described in *Materials and Methods*. DIC images of the indicated strains are shown in left panels, and anti-Pma1p immunofluorescence (IF) in the same cells is shown in the right panels.

If mislocalization of Stv1p in the class E *vps* mutants accounts for the synthetic Vma⁻ phenotype with the *rav1Δ* mutation, then other mutations with a similar synthetic growth phenotype may also affect Stv1p localization. A number of mutants other than class E *vps* mutants exhibit a synthetic Vma⁻ phenotype with *rav1Δ* (Table S1). Growth assays for two of these mutants, *vps53Δ* and *ubp3Δ*, alone and in combination with *rav1Δ*, are shown in Figure 8A. Double mutants with *rav1Δ* grow well on YEPD buffered to pH 5, but grow poorly on YEPD, pH 7.5 +$CaCl_2$ medium at 30°C, indicating the synthetic Vma⁻ phenotype. *VPS53* encodes a component of the GARP (Golgi-associated retrograde protein) complex that is required for retrograde sorting of proteins from endosomes to the Golgi apparatus; several other components of this complex were identified in our SGA screen as well as in previous screens (Table S1). *UBP3* is a deubiquitinating enzyme that has been implicated in multiple processes, including regulation of transport between the ER and Golgi apparatus. We found evidence of Stv1p-GFP mislocalization in the *vps53Δ* and *ubp3Δ* single mutants (Figure 8B). In the *vps53Δ* mutant, Stv1p-GFP appears to have a reticular distribution. In the *ubp3Δ* mutant, Stv1p-GFP is present in the vacuolar membrane of ~50% of cells. These results support the conclusion that the synthetic genetic analysis with *rav1Δ* has uncovered novel mutations with roles in Stv1p localization.

DISCUSSION

The RAVE complex as an isoform-specific assembly factor

V-ATPases are ubiquitous in eukaryotic cells, and subunit isoforms are believed to impart not only tissue specificity, but also distinct localization, biochemical features, and regulation to the multiple V-ATPases present in a single cell (Toyomura *et al.*, 2000; Sun-Wada *et al.*, 2003; Hurtado-Lorenzo *et al.*, 2006; Pietrement *et al.*, 2006; Forgac, 2007; Blake-Palmer and Karet, 2009). The V_o *a* subunits, in particular, have been shown to contain essential targeting information (Manolson *et al.*, 1994; Toyomura *et al.*, 2003; Finnigan *et al.*, 2012), and to govern coupling and disassembly behavior of V-ATPases (Kawasaki-Nishi *et al.*, 2001a). There is limited information about how different isoforms bestow these differences on V-ATPases. This work suggests that differential interactions with the RAVE complex may support at least some of the distinct features of the yeast Vph1p- and Stv1p-containing V-ATPases.

Vph1p is expressed at much higher levels than Stv1p and is responsible for vacuolar acidification, so loss of vacuolar pH control

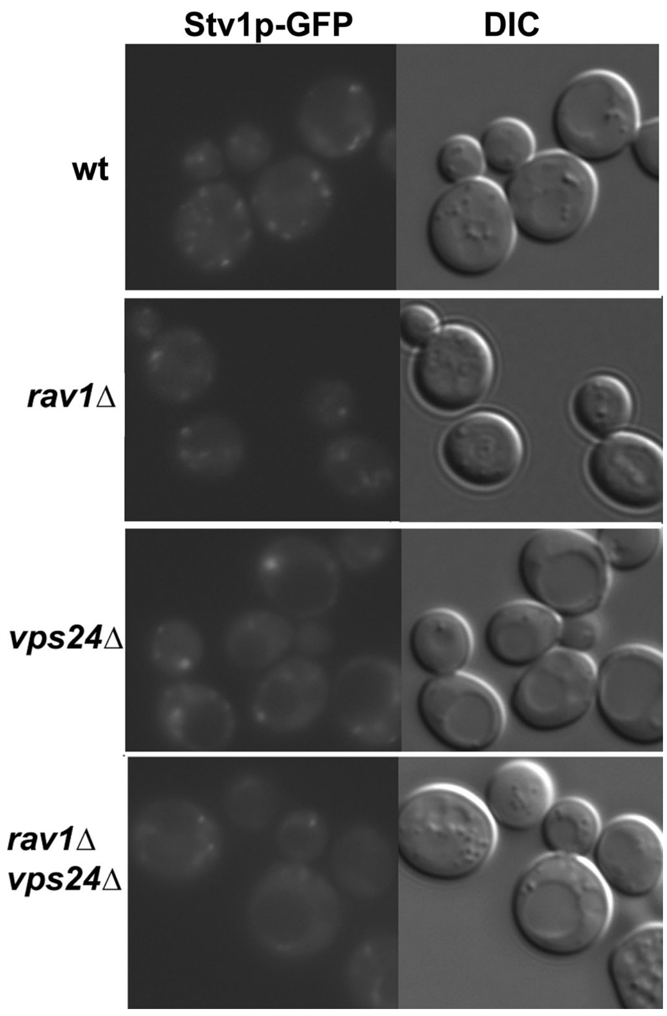

FIGURE 7: Stv1p-GFP localization in wild-type, *vps24Δ*, *rav1Δ*, and *vps24Δrav1Δ*. Localization of Stv1p-GFP in the indicated strains was visualized by fluorescence microscopy under GFP optics (left) and under DIC (right).

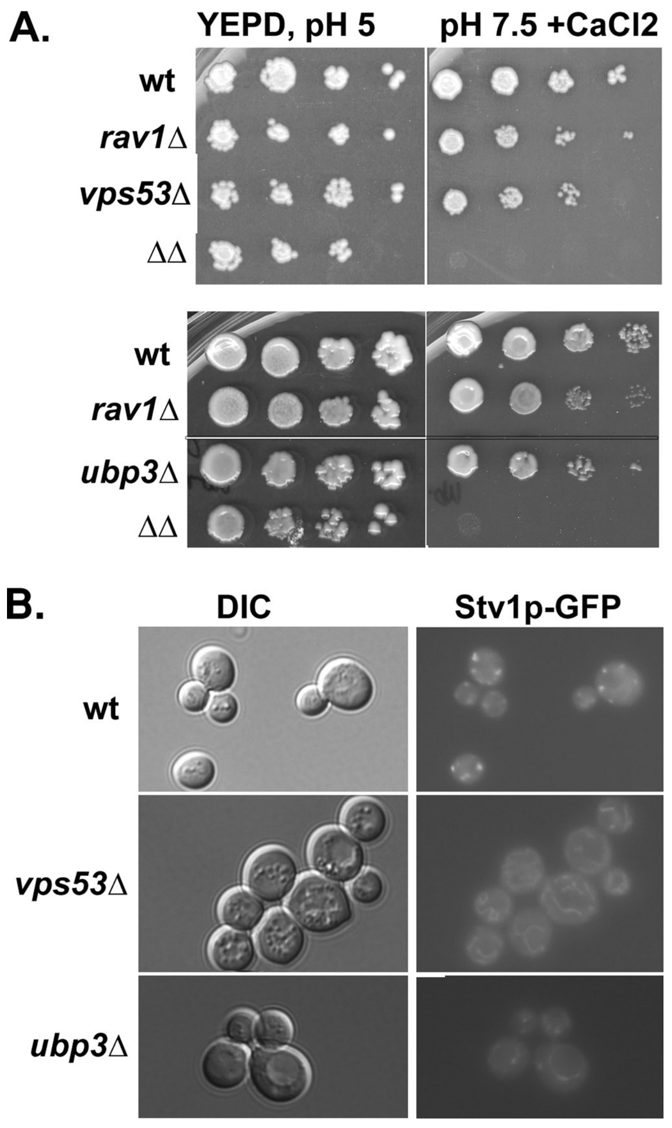

FIGURE 8: Other mutants that show synthetic Vma⁻ growth phenotypes with *rav1Δ* also perturb Stv1p-GFP localization. (A) Growth of the four spores from single tetrads derived from diploids heterozygous for *rav1Δ* and either *ubp3Δ* (PKY105-4A-D) or *vps53Δ* (PKY100-5A-D) are compared on YEPD, pH 5 and YEPD, pH 7.5 + 60 mM $CaCl_2$ after growth at 30°C as in Figure 1. (B) Localization of Stv1p-GFP in wild-type, *ubp3Δ*, and *vps53Δ* cells was visualized as in Figure 7.

indicates defects in Vph1p-containing V-ATPases (Manolson *et al.*, 1994; Tarsio *et al.*, 2011; Finnigan *et al.*, 2012). Although it has been known for some time that isolated *rav1Δ* and *rav2Δ* vacuoles have very low ATPase activity in isolated vacuoles (Smardon *et al.*, 2002; Smardon and Kane, 2007), the partial Vma⁻ phenotype of these mutants had suggested that V-ATPases might be somewhat active in vivo but unstable, resulting in loss of activity during vacuole isolation. The vacuolar pH measurements in Figure 2 make it clear that vacuolar acidification is severely defective in the *rav1Δ* mutant in vivo, and in fact, comparable with a *vph1Δ* mutant (Tarsio *et al.*, 2011). This indicates that RAVE function is essential for activity of Vph1p-containing V-ATPases at the vacuole. When expressed at endogenous levels, Stv1p never reaches the vacuole and thus does not contribute to vacuolar acidification (Tarsio *et al.*, 2011; Finnigan *et al.*, 2012). Overexpression of *STV1* saturates a sorting step and allows transport to the vacuole, where it partially suppresses the defects of a *vph1Δ* mutant (Finnigan *et al.*, 2012). Suppression of the functional and biochemical defects of a *rav1Δ* mutation by *STV1* indicates that Stv1p-containing V-ATPases do not require RAVE for function, and increased assembly of peripheral V_1 subunits at the vacuolar membrane in a *rav1Δ* strain overexpressing *STV1* confirms that these complexes can assemble in the absence of RAVE (Figure 3). Thus RAVE appears to be the first Vph1p isoform-specific assembly factor.

Figures 4 and 5 provide the first evidence of any interaction between the RAVE complex and the V_o membrane sector of the V-ATPase and are entirely consistent with the role of RAVE in reassembly of dissociated V_1 and V_o subcomplexes. The N-terminal domains of Stv1p and Vph1p are exposed to the cytosol and are required for a number of critical interactions with the V_1 sector in the assembled V-ATPase (Benlekbir *et al.*, 2012; Oot and Wilkens, 2012). The Rav1p subunit of RAVE has previously been shown to interact with multiple V_1 subunits, including subunits E, G, and C (Smardon *et al.*, 2002; Smardon and Kane, 2007). The Skp1p subunit of the complex has been implicated in release of RAVE from the membrane (Brace *et al.*, 2006). However, these interactions provide little insight into how RAVE might act as an assembly factor. An interaction between Rav1p and Vph1-NT suggests that the RAVE complex may be positioned to promote assembly by bringing the disassembled C subunit, V_1 and V_o subcomplexes into proximity, perhaps assisted by Skp1p acting as a membrane tether. Interestingly, Stv1p-containing V-ATPases show less disassembly in response to glucose deprivation than Vph1p-containing complexes (Kawasaki-Nishi *et al.*, 2001a,b), so the RAVE dependence of Vph1p is entirely consistent with the role of RAVE in reversible disassembly. The differences in interaction of the N-terminal domains of Vph1p and Stv1p (Vph1-NT and Stv1-NT) with Rav1p in the two-hybrid assay support the functional preference of the RAVE complex for Vph1p- over Stv1p-containing complexes (Figure 4). However, while we provide strong functional evidence that Stv1p-containing complexes do not require RAVE, further investigation is required to demonstrate whether and how RAVE distinguishes Vph1p from Stv1p at a biochemical level.

It is not yet known whether subunit *a* isoforms in higher eukaryotes show variations in RAVE dependence. Loss of rabconnectin function has been shown to severely reduce acidification of late endosomes in *Drosophila* follicle cells and eye disks (Yan *et al.*, 2009) and to eliminate synaptic vesicle acidification in zebrafish hair cells (Einhorn *et al.*, 2012). Notably, the zebrafish *stardust* alleles contain nonsense mutations in the single rabconnectin α gene predicted to delete as much as 70% of the protein (Einhorn *et al.*, 2012), but do not result in as severe a phenotype as knockdowns of V-ATPase subunits (Horng *et al.*, 2007). This might suggest that some level of V-ATPase activity persists in the absence of rabconnectin α function. Although the V-ATPase subunit *a* isoform specificity has not been analyzed in the fly, zebrafish, or mouse cell compartments, where defects in rabconnectin-dependent organelle acidification and/or V-ATPase assembly were documented, previous data suggest that synaptic vesicles are generally enriched in the *a1* isoform (Hiesinger *et al.*, 2005), while late endosomes (and lysosomes) predominantly carry the *a3* isoform (Toyomura *et al.*, 2003).

Is yeast RAVE necessary for functions other than vacuolar acidification?

Given the lack of vacuolar acidification in the RAVE mutants, we would anticipate that the relatively mild phenotype of the *rav1Δ* and *rav2Δ* mutants must be supported by acidification of other compartments. These mild phenotypes, coupled with the ability of Stv1p-containing complexes to assemble at the vacuole, suggest that Stv1p-containing complexes may be capable of RAVE-independent assembly and function in other compartments. The synthetic Vma⁻ phenotype of the *rav1Δstv1Δ* mutant (Figure 6A) supports this. However, there is evidence that RAVE function is required for more than vacuolar acidification. Morphological alterations in endosomes and defects in potential endosome-related functions have been observed in yeast *rav1* mutants (Sipos *et al.*, 2004; Brace *et al.*, 2006) and higher eukaryotes lacking rabconnectin function (Yan *et al.*, 2009), suggesting a requirement for RAVE in endosomal compartments. In yeast, these defects might be attributed to defective assembly of Vph1p-containing V-ATPases en route to the vacuole, consistent with RAVE dependence of Vph1p-containing complexes at the vacuole. However, the phenotypes of *rav1Δ* and *vph1Δ* mutants are not identical; specifically, the temperature-sensitive phenotype of the *rav1Δ* mutant is not shared by *vph1Δ*. In addition, Figure 3C suggests levels of Vph1p may be somewhat higher in *rav1Δ* vacuoles than in wild-type cells, which could indicate an altered distribution of Vph1-containing V_o complexes in the mutant that is resolved in the *STV1*-overexpressing strain. Further experiments are necessary to elucidate the full range of RAVE function.

Synthetic Vma⁻ phenotypes with *rav1Δ* define mutations affecting Stv1p localization

If RAVE function is directed primarily at Vph1p-containing V-ATPases, then it follows that mutations that cause synthetic Vma⁻ phenotypes in combination with *rav1Δ* may affect Stv1p function. Consistent with this hypothesis, the class E *vps* mutants, identified by their synthetic Vma⁻ phenotypes with *rav1Δ* in our screen, were previously shown to affect Stv1p localization. Although the steady-state localization of Stv1p in wild-type cells is predominantly in the Golgi, in a class E mutant, Stv1p accumulates in the class E compartment adjacent to the vacuole and appears to be depleted from the Golgi (Kawasaki-Nishi *et al.*, 2001a). This localization reflects a requirement for ongoing traffic between the endosome and Golgi apparatus, because a *vps26Δ* mutant, which disrupts retromer function and prevents retrograde transport from endosome to Golgi, also accumulates Stv1p in late endosomes (Finnigan *et al.*, 2011). The functional consequences of halting Stv1p retrograde transport have not been fully explored, but significantly, a reconstructed "ancestral *a* subunit" that does not undergo retrograde transport is not able to grow under low-iron conditions, wherein V-ATPase function in the Golgi may become critical (Finnigan *et al.*, 2011). We hypothesize that, in our screen, the class E *vps* mutants reduced the population of Stv1p-containing complexes engaging in retrograde transport. The consequences of this depletion were observed only when the activity of Vph1p-containing complexes was lost through the *rav1Δ* mutation. Given the alterations of endosome morphology and trafficking reported previously for the *rav1Δ* mutant, we cannot eliminate the possibility that the *rav1Δ* mutation directly or indirectly compromises Stv1p localization, but any Stv1p defect in the *rav1Δ* mutant must be too subtle to generate a defect in growth or Pma1p localization.

The endosome to Golgi retrograde targeting signal on Stv1p was recently identified (Finnigan *et al.*, 2012), but the apparatus responsible for recognizing this signal has not been identified. If our interpretation of the *rav1Δ* synthetic lethality screen is correct, we would predict that additional proteins responsible for Stv1p signal recognition and transport are likely to be among the mutations that generate a synthetic Vma⁻ phenotype in combination with *rav1Δ*. Further experiments are necessary to fully characterize this isoform-specific sorting machinery.

MATERIALS AND METHODS

Strains

Supplemental Table S3 lists the yeast strains described in this work. The yeast nonessential deletion mutant array in the BY4741 background was purchased from Research Genetics/Open Biosystems (Thermo Scientific, Denver, CO). The *rav1Δ::nat*^{R} allele, consisting of ~400 base pairs upstream and ~300 base pairs downstream of *RAV1* surrounding the natMX cassette, was constructed by fusion PCR and transformed into yeast strain Y3656 (Tong *et al.*, 2004; provided by Charlie Boone, University of Toronto). The S288C *STV1*-GFP strain was purchased from Invitrogen (Grand Island, NY), and the *STV1-GFP-HIS3* cassette was PCR-amplified with oligonucleotides STV1 2391ORF (5′-GGCACTATCGTTGGCGCATG-3′) and STV1+500 (5′-TACAGCAGAGATTTATGGTATGCC-3′). The PCR product was then transformed into the *rav1Δ*, *vps24Δ*, *rav1Δvps24Δ*, *ubp3Δ*, and *vps53Δ* strains. HA-tagged *STV1* in a 2-micron vector (YEp352; Kawasaki-Nishi *et al.*, 2001b) was a generous gift from Michael Forgac (Tufts University). The BY4741 *vph1Δ::kanMX stv1Δ::nat*^{R} strain was prepared by switching the kanMX marker in *stv1Δ::kanMX* to *natMX* as described previously (Tong *et al.*, 2001), amplifying the resulting *stv1Δ::nat*^{R} allele by PCR with oligonucleotides STV1+500 (above) and STV1-500 (5′-GTTTTCCATCAAACTGGCTAGTTT-3′), and introducing this allele into the BY4741 *vph1Δ::kanMX* strain.

Yeast strains were maintained on YEPD medium buffered to pH 5 with 50 mM sodium phosphate and 50 mM sodium succinate or fully supplemented minimal medium (SC) as indicated. For serial-dilution growth assays, log-phase cultures were diluted to the same density in growth medium, and 10-fold serial dilutions into medium were made. Cells were then transferred to the indicated plates using a pinning tool. YEPD, pH 7.5 plates were buffered to pH 7.5 with 50 mM sodium phosphate, 50 mM sodium succinate; YEPD, pH 7.5 + $CaCl_2$ plates were buffered with 50 mM MES, 50 mM MOPS and contained 60 mM calcium chloride. Selection plates for two-hybrid assays were prepared as described previously (James *et al.*, 1996).

SGA

SGA was performed as described previously (Tong *et al.*, 2001) using a Virtek pinning robot at all steps. Briefly, the Y3656 *rav1Δ* mutant was mated to the deletion mutant array (384 colonies/plate format) on YEPD, and then diploids were selected on YEPD containing 0.1 mg/ml clonNAT (Werner Biosciences, Jena, Germany) and 0.2 mg/ml G418 sulfate (US Biological). The diploids were next pinned onto sporulation medium (Kassir and Simchen, 1991) and incubated for ~11 d at 30°C. After sporulation, colonies were pinned two consecutive times to SC medium lacking histidine and arginine and containing 0.07 mg/ml canavanine (haploid select medium) and grown for 4–5 d to select for *MATa* spores. (For all SC plates used for SGA, yeast nitrogen base lacking amino acids and ammonium sulfate was used, and 1 g/l of monosodium glutamate was added; Tong *et al.*, 2001.) From the second set of haploid selection plates, colonies were pinned to one set of haploid selection plates containing 0.02 mg/ml G418 (which selects for the deletion library mutation only) and another set of haploid selection plates containing 0.02 mg/ml G418 and 0.01 mg/ml clonNAT (which selects for double mutants). The single- and double-mutant selection plates were screened by visual inspection after growth for 2 d at 30°C. Strains that showed poorer growth on the double-mutant selection plates relative to the single-mutant selection plates were identified as candidates for synthetic genetic interactions. The entire SGA protocol was repeated three times, and only candidates that were identified in two of the three independent screens are included in Table S1. Biological process and cellular component GO terms for the candidate mutations showing interactions with *rav1Δ* by SGA were obtained by submitting the genes in Table S1 to FunSpec (Robinson *et al.*, 2002).

Confirmation of candidate synthetic interactions from SGA

Candidate interactions were confirmed by tetrad dissection or plasmid shuffle. For tetrad dissections, the Y3656 *rav1Δ* mutant was mated to the candidate mutant in the BY4741 background. After selection of diploids on YEPD containing G418 and clonNAT, the diploids were sporulated in liquid medium, and then tetrads were dissected on YEPD, pH 5 plates and grown at 30°C. Spores were genotyped by testing growth on G418 and ClonNAT-containing plates. Growth of the spores on YEPD, pH 5; YEPD, pH 7.5; YEPD, pH 7.5+ 60 mM $CaCl_2$; and SC at 30 and 37°C was then compared to look for synthetic phenotypes. Strains HDY13-9A, HDY13-9B, HDY13-9C, and HDY13-9D, derived from a single tetrad, were used in comparisons of wild-type, *vps24Δ*, *rav1Δ*, and *rav1Δvps24Δ* strains in Figures 1, 2, and 5. For plasmid shuffle, the library deletion was transformed with wild-type *RAV1* on a *URA3*-marked plasmid, and the resulting strain was transformed with a *rav1Δ::LEU2* allele as described (Smardon *et al.*, 2002). The plasmid was then evicted by growth on medium containing 5-fluoroorotic acid, which counterselects against the *URA3*-marked plasmid, and the resulting double mutants were characterized.

Vacuolar pH and V-ATPase characterization

Vacuolar pH was measured using 2′,7′-bis-(2-carboxyethyl)-5-(and-6)-carboxyfluorescein, acetoxymethyl ester (BCECF-AM; Invitrogen/Life Technologies, Grand Island, NY) as described previously (Martinez-Munoz and Kane, 2008; Tarsio *et al.*, 2011). Vacuolar vesicles were isolated from Y3656 *rav1Δ* cells grown to log phase in either SC or SC lacking uracil (to maintain the *STV1* overexpression plasmid), buffered to pH 5 with 50 mM MES (2-(*N*-morpholino)ethanesulfonic acid; Diakov and Kane, 2010). ATP hydrolysis was measured in the presence and absence of 100 nM concanamycin A (Sigma-Aldrich, Piscataway, NJ), and concanamycin-sensitive ATPase activity was taken as the V-ATPase activity. For immunoblots, total vacuolar protein in each sample was measured by Lowry assay, and equal amounts of vacuolar protein from each strain were separated by SDS–PAGE. After transfer of protein to nitrocellulose, blots were probed with the following antibodies: monoclonal antibodies 10D7, 8B1, 13D11, and 7A2, against V-ATPase subunits Vph1p, Vma1p, Vma2p, and Vma5p, respectively; HA.11 (Covance, Princeton, NJ) against the HA epitope; and 1D3 (Invitrogen) against yeast alkaline phosphatase; all probes were subsequently detected with alkaline phosphatase–conjugated goat anti-mouse antibody (Promega, Madison, WI). Whole-cell lysates were prepared as described previously (Kane *et al.*, 1992), except that lysis was performed at 95°C.

Two-hybrid analysis

To introduce STV1-NT into the pACT two-hybrid plasmid (Harper *et al.*, 1993), we amplified the open reading frame encoding the first 454 amino acids of Stv1 from wild-type genomic DNA with primer pair STV12H-5p (GCGGATCCTCATGAATCAAGAAGAGGCTATATTCCG) and STV1 2H-3p (GCCTCGAGACCAGCATTGATTTCTTTATATGTTGCG). A *Bam*HI site was introduced just upstream of the ATG start codon and in frame with the activation domain of the pACT plasmid. The resulting PCR fragment was cloned into the pGEM T-Easy cloning vector (Promega) and sequenced for accuracy. The STV1-NT insert was excised using *Bam*HI and *Xho*1 and cloned into the *Bam*HI/*Xho*1-cleaved pACT vector. Construction of pACT-VPH1-NT containing the first 409 amino acids of Vph1p and pAS-RAV1 containing the entire *RAV1* open reading frame were previously described (Smardon and Kane, 2007; Diab *et al.*, 2009). The pACT, pACT-VPH1-NT, and pACT-STV1-NT plasmids were transformed into the PJ69-4α (*MAT*α) strain (James *et al.*, 1996). Transformants were selected on SC plates lacking tryptophan to select for the pAS-RAV1 plasmid and SC plates lacking leucine to select for the pACT plasmids. For testing for two-hybrid interactions, the *MATa* strain (PJ69-4A) containing the pAS-RAV1 plasmid was crossed separately to each of the *MAT*α strains containing either the pACT vector alone, the pACT-VPH1-NT, or the pACT-STV1-NT, and diploids were selected on SC –Trp, –Leu plates. The resulting diploid strains were tested for two-hybrid interactions by streaking onto SD –Trp, –Leu, –His, –Ade plates to test for expression of the *HIS3* and *ADE2* two-hybrid reporter genes.

Bacterial expression of Vph1-NT and Rav1(840–1125)

Construction of maltose-binding protein (MBP)-tagged Vph1-NT (corresponding to the first 406 amino acids of Vph1p) in pMalpAse has been described previously (Diab *et al.*, 2009). This plasmid was mutagenized to add a FLAG tag to the C-terminus of Vph1NT by inverse PCR using oligonucleotides 5′-CAGAGAAATCAATGACTATAAAGACGACGATGACAA-3′ and 5′-GTCTTTATAGTCATTGATTTCTCTGTACTGAGCAAT-3′. The tagged construct was confirmed by sequencing. The plasmid pGST-Rav1(840–1125) was created by first amplifying the region of *RAV1* between amino acids 840–1125 using the oligos RAV1-CT2H (5′-GGCCAGATCTTCCTTACTGAGCAACTAACGAAAACAAC-3′) and RAV1CT-Sal (5′-GCGTCGACGAAACAATGCTTGAGTTGTTTTCTAAATC-3′). *Bgl*II and *Sal*I sites are underlined in the respective oligos. The amplified product was cloned into the pCR4Blunt-TOPO plasmid (Invitrogen) following the supplier's protocol. The *Bgl*II-*Sal*I fragment was cleaved from this plasmid in a double digest, gel extracted, and cloned into the pET-41c(+) plasmid (Novagen) in frame with an N-terminal GST tag.

MBP-Vph1NT-FLAG was expressed in BL21 cells after overnight induction with 0.3 mM isopropyl-β-D-1-thiogalactopyranoside at 19°C. GST-Rav1(840–1125) was also expressed in BL21 cells, but with an induction time of 3 h at 37°C. After cell lysis, the MBP-Vph1NT-FLAG fusion was purified by passage through an amylose column (New England Biolabs, Ipswich, MA), and the eluted fractions were cleaved overnight with Prescission protease. The cleaved protein was passed through an anti-FLAG M2 column and washed with column buffer (20 mM Tris-HCl, 150 mM NaCl, and 1 mM EDTA, pH 7.2), and Vph1NT-FLAG was eluted with 100 µg/ml FLAG peptide. GST-Rav1(840–1125) from a cell lysate was bound to glutathione resin (GenScript, Piscataway, NJ), and the resin was washed with 20 column volumes of phosphate-buffered saline (137 mM NaCl, 2.6 mM KCl, 12 mM Na_2HPO_4, pH 7.2). Glutathione beads with the bound GST-Rav1(840–1125) were then incubated with purified Vph1NT-FLAG for 3 h at 4°C. The beads were then washed with the same buffer, and then the bound proteins were eluted with 10 mM glutathione.

Fluorescence microscopy

Pma1p was visualized by indirect immunofluorescence using the 40B7 monoclonal antibody (Abcam, Cambridge, MA) followed by Alexa Fluor 488–conjugated goat anti-mouse antibody (Invitrogen) as described previously (Tarsio *et al.*, 2011). For visualization of Stv1p-GFP, cells were grown to log phase in SC buffered to pH 5 with 50 mM MES and then visualized directly. All samples were visualized on a Zeiss Imager.Z1 fluorescence microscope equipped with a Hamamatsu CCD camera and AxioVision software. Micrographs were assembled into figures using Adobe Photoshop CS4, ver. 11.0.2.

ACKNOWLEDGMENTS

This work was supported by National Institutes of Health grants R01 GM50322 and R01 GM63742 to P.M.K. The authors thank Charlie Boone, Masashi Ohira, and Michael Forgac for reagents; David Amberg for advice on SGA screening; and Michael James, Joseph Harrison, and Amanjot Grewal for technical assistance on the project.

REFERENCES

Benlekbir S, Bueler SA, Rubinstein JL (2012). Structure of the vacuolar-type ATPase from *Saccharomyces cerevisiae* at 11-A resolution. Nat Struct Mol Biol 19, 1356–1362.

Blake-Palmer KG, Karet FE (2009). Cellular physiology of the renal H^+ATPase. Curr Opin Nephrol Hypertens 18, 433–438.

Bowers K, Lottridge J, Helliwell SB, Goldthwaite LM, Luzio JP, Stevens TH (2004). Protein-protein interactions of ESCRT complexes in the yeast *Saccharomyces cerevisiae*. Traffic 5, 194–210.

Brace EJ, Parkinson LP, Fuller RS (2006). Skp1p regulates Soi3p/Rav1p association with endosomal membranes but is not required for vacuolar ATPase assembly. Eukaryot Cell 5, 2104–2113.

Chatr-Aryamontri A *et al.* (2013). The BioGRID interaction database: 2013 update. Nucleic Acids Res 41, D816–D823.

Costanzo M *et al.* (2010). The genetic landscape of a cell. Science 327, 425–431.

Diab H, Ohira M, Liu M, Cobb E, Kane PM (2009). Subunit interactions and requirements for inhibition of the yeast V1-ATPase. J Biol Chem 284, 13316–13325.

Diakov TT, Kane PM (2010). Regulation of vacuolar proton-translocating ATPase activity and assembly by extracellular pH. J Biol Chem 285, 23771–23778.

Einhorn Z, Trapani JG, Liu Q, Nicolson T (2012). Rabconnectin3α promotes stable activity of the H^+ pump on synaptic vesicles in hair cells. J Neurosci 32, 11144–11156.

Finnigan GC, Cronan GE, Park HJ, Srinivasan S, Quiocho FA, Stevens TH (2012). Sorting of the yeast vacuolar-type, proton-translocating ATPase enzyme complex (V-ATPase): identification of a necessary and sufficient Golgi/endosomal retention signal in Stv1p. J Biol Chem 287, 19487–19500.

Finnigan GC, Hanson-Smith V, Houser BD, Park HJ, Stevens TH (2011). The reconstructed ancestral subunit a functions as both V-ATPase isoforms Vph1p and Stv1p in *Saccharomyces cerevisiae*. Mol Biol Cell 22, 3176–3191.

Forgac M (2007). Vacuolar ATPases: rotary proton pumps in physiology and pathophysiology. Nat Rev Mol Cell Biol 8, 917–929.

Harper JW, Adami GR, Wei N, Keyomarsi K, Elledge SJ (1993). The p21 Cdk-interacting protein Cip1 is a potent inhibitor of G1 cyclin-dependent kinases. Cell 75, 805–816.

Hiesinger PR *et al.* (2005). The v-ATPase V_0 subunit a1 is required for a late step in synaptic vesicle exocytosis in *Drosophila*. Cell 121, 607–620.

Hirata T, Iwamoto-Kihara A, Sun-Wada GH, Okajima T, Wada Y, Futai M (2003). Subunit rotation of vacuolar-type proton pumping ATPase: relative rotation of the G and C subunits. J Biol Chem 278, 23714–23719.

Horng JL, Lin LY, Huang CJ, Katoh F, Kaneko T, Hwang PP (2007). Knockdown of V-ATPase subunit A (atp6v1a) impairs acid secretion and ion balance in zebrafish (*Danio rerio*). Am J Physiol Regul Integr Comp Physiol 292, R2068–R2076.

Hurley JH, Emr SD (2006). The ESCRT complexes: structure and mechanism of a membrane-trafficking network. Annu Rev Biophys Biomol Struct 35, 277–298.

Hurtado-Lorenzo A *et al.* (2006). V-ATPase interacts with ARNO and Arf6 in early endosomes and regulates the protein degradative pathway. Nat Cell Biol 8, 124–136.

James P, Halladay J, Craig EA (1996). Genomic libraries and a host strain designed for highly efficient two-hybrid selection in yeast. Genetics 144, 1425–1436.

Kane PM (2000). Regulation of V-ATPases by reversible disassembly. FEBS Lett 469, 137–141.

Kane PM (2006). The where, when, and how of organelle acidification by the yeast vacuolar H^+-ATPase. Microbiol Mol Biol Rev 70, 177–191.

Kane PM (2007). The long physiological reach of the yeast vacuolar H^+-ATPase. J Bioenerg Biomembr 39, 415–421.

Kane PM, Kuehn MC, Howald-Stevenson I, Stevens TH (1992). Assembly and targeting of peripheral and integral membrane subunits of the yeast vacuolar H^+-ATPase. J Biol Chem 267, 447–454.

Kassir Y, Simchen G (1991). Monitoring meiosis and sporulation in *Saccharomyces cerevisiae*. Methods Enzymol 194, 94–110.

Katzmann DJ, Stefan CJ, Babst M, Emr SD (2003). Vps27 recruits ESCRT machinery to endosomes during MVB sorting. J Cell Biol 162, 413–423.

Kawasaki-Nishi S, Bowers K, Nishi T, Forgac M, Stevens TH (2001a). The amino-terminal domain of the vacuolar proton-translocating ATPase a subunit controls targeting and in vivo dissociation, and the carboxyl-terminal domain affects coupling of proton transport and ATP hydrolysis. J Biol Chem 276, 47411–47420.

Kawasaki-Nishi S, Nishi T, Forgac M (2001b). Yeast V-ATPase complexes containing different isoforms of the 100-kDa a-subunit differ in coupling efficiency and in vivo dissociation. J Biol Chem 276, 17941–17948.

Kraemer C, Weil B, Christmann M, Schmidt ER (1998). The new gene *DmX* from *Drosophila melanogaster* encodes a novel WD-repeat protein. Gene 216, 267–276.

Manolson MF, Proteau D, Preston RA, Stenbit A, Roberts BT, Hoyt MA, Preuss D, Mulholland J, Botstein D, Jones EW (1992). The VPH1 gene encodes a

95-kDa integral membrane polypeptide required for in vivo assembly and activity of the yeast vacuolar H^+-ATPase. J Biol Chem 267, 14294–14303.
Manolson MF, Wu B, Proteau D, Taillon BE, Roberts BT, Hoyt MA, Jones EW (1994). STV1 gene encodes functional homologue of 95-kDa yeast vacuolar H^+-ATPase subunit Vph1p. J Biol Chem 269, 14064–14074.
Martinez-Munoz GA, Kane P (2008). Vacuolar and plasma membrane proton pumps collaborate to achieve cytosolic pH homeostasis in yeast. J Biol Chem 283, 20309–20319.
Nagano F, Kawabe H, Nakanishi H, Shinohara M, Deguchi-Tawarada M, Takeuchi M, Sasaki T, Takai Y (2002). Rabconnectin-3, a novel protein that binds both GDP/GTP exchange protein and GTPase-activating protein for Rab3 small G protein family. J Biol Chem 277, 9629–9632.
Oot RA, Wilkens S (2012). Subunit interactions at the V_1-V_o interface in yeast vacuolar ATPase. J Biol Chem 287, 13396–13406.
Pietrement C, Sun-Wada GH, Silva ND, McKee M, Marshansky V, Brown D, Futai M, Breton S (2006). Distinct expression patterns of different subunit isoforms of the V-ATPase in the rat epididymis. Biol Reprod 74, 185–194.
Piper RC, Cooper AA, Yang H, Stevens TH (1995). VPS27 controls vacuolar and endocytic traffic through a prevacuolar compartment in *Saccharomyces cerevisiae*. J Cell Biol 131, 603–617.
Qi J, Forgac M (2007). Cellular environment is important in controlling V-ATPase dissociation and its dependence on activity. J Biol Chem 282, 24743–24751.
Raymond CK, Howald-Stevenson I, Vater CA, Stevens TH (1992). Morphological classification of the yeast vacuolar protein sorting mutants: evidence for a prevacuolar compartment in class E *vps* mutants. Mol Biol Cell 3, 1389–1402.
Robinson MD, Grigull J, Mohammad N, Hughes TR (2002). FunSpec: a web-based cluster interpreter for yeast. BMC Bioinformatics 3, 35.
Sakisaka T, Takai Y (2005). Purification and properties of rabconnectin-3. Methods Enzymol 403, 401–407.
Seol JH, Shevchenko A, Deshaies RJ (2001). Skp1 forms multiple protein complexes, including RAVE, a regulator of V-ATPase assembly. Nat Cell Biol 3, 384–391.
Sethi N, Yan Y, Quek D, Schupbach T, Kang Y (2010). Rabconnectin-3 is a functional regulator of mammalian Notch signaling. J Biol Chem 285, 34757–34764.
Sipos G, Brickner JH, Brace EJ, Chen L, Rambourg A, Kepes F, Fuller RS (2004). Soi3p/Rav1p functions at the early endosome to regulate endocytic trafficking to the vacuole and localization of *trans*-Golgi network transmembrane proteins. Mol Biol Cell 15, 3196–3209.
Smardon AM, Kane PM (2007). RAVE is essential for the efficient assembly of the C subunit with the vacuolar H^+-ATPase. J Biol Chem 282, 26185–26194.
Smardon AM, Tarsio M, Kane PM (2002). The RAVE complex is essential for stable assembly of the yeast V-ATPase. J Biol Chem 277, 13831–13837.
Sun-Wada GH, Yoshimizu T, Imai-Senga Y, Wada Y, Futai M (2003). Diversity of mouse proton-translocating ATPase: presence of multiple isoforms of the C, d and G subunits. Gene 302, 147–153.
Tarsio M, Zheng H, Smardon AM, Martinez-Munoz GA, Kane PM (2011). Consequences of loss of Vph1 protein-containing vacuolar ATPases (V-ATPases) for overall cellular pH homeostasis. J Biol Chem 286, 28089–28096.
Tong AH *et al*. (2001). Systematic genetic analysis with ordered arrays of yeast deletion mutants. Science 294, 2364–2368.
Tong AH *et al*. (2004). Global mapping of the yeast genetic interaction network. Science 303, 808–813.
Toyomura T, Murata Y, Yamamoto A, Oka T, Sun-Wada GH, Wada Y, Futai M (2003). From lysosomes to the plasma membrane: localization of vacuolar-type H^+-ATPase with the a_3 isoform during osteoclast differentiation. J Biol Chem 278, 22023–22030.
Toyomura T, Oka T, Yamaguchi C, Wada Y, Futai M (2000). Three subunit *a* isoforms of mouse vacuolar H^+-ATPase. Preferential expression of the a_3 isoform during osteoclast differentiation. J Biol Chem 275, 8760–8765.
Yan Y, Denef N, Schupbach T (2009). The vacuolar proton pump, V-ATPase, is required for notch signaling and endosomal trafficking in *Drosophila*. Dev Cell 17, 387–402.